Seminars in Vascular Surgery xxx (2019) 1–12

Available online at www.sciencedirect.com

ScienceDirect

www.elsevier.com/locate/semvascsurg

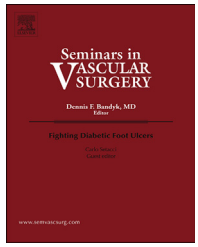

Geometrical changes in Anaconda endograft limbs after endovascular aneurysm repair: A potential predictor for limb occlusion

Jaimy A. Simmering [a,b,*], *Robert H. Geelkerken* [a,b], *Cornelis H. Slump* [c], *and Maaike A. Koenrades* [a,b,c]

[a] *Department of Vascular Surgery, Medisch Spectrum Twente, Enschede, The Netherlands*
[b] *Multimodality Medical Imaging M3i Group, Faculty of Science and Technology, Technical Medical Centre, University of Twente, PO Box 217, 7500 AE Enschede, The Netherlands*
[c] *Robotics and Mechatronics Group, Faculty of Electrical Engineering, Mathematics and Computer Science, Technical Medicine Centre, University of Twente, Enschede, The Netherlands*

ARTICLE INFO

ABSTRACT

The emergence of limb occlusion after endovascular aneurysm repair may be related to the conformational changes between the endograft structure and the patient's anatomy. This study analyzed detailed geometric changes of Anaconda endograft (Terumo Aortic, Inchinnan, Scotland, UK) limbs during the cardiac cycle–based computed tomography on serial imaging after graft implantation. Fifteen patients (mean age 72.8 ± 3.7 years; 14 men) underwent postoperative electrocardiogram-gated computed tomography scans according to a prospective study design between April 2014 and May 2017. Changes in curvature, length of the limbs, and distances between successive stent rings (inter-ring distance) of the endograft limbs during a 2-year follow-up period were quantified using meticulous image processing methods involving image registration, centerline extraction, and model-based stent-ring segmentation. From discharge to 24 months, mean curvature increased significantly by 9.6 m^{-1} (standard deviation [SD], 11.1 m^{-1}; 95% confidence interval [CI], 3.4 to 15.8 m^{-1}; $P = .002$) for the right limbs and by 6.1 m^{-1} (SD 9.4 m^{-1}; 95% CI, 0.8 to 11.5 m^{-1}; $P = .21$) for the left limbs. The length of the right limbs decreased significantly, by 9.5 mm (SD 7.6 mm; 95% CI, 3.5 to 15.6 mm; $P = .002$); the length of the left limbs decreased by 10.1 mm (SD 5.1 mm; 95% CI, 5.9 to 14.2 mm; $P < .001$). The minimal inter-ring distance decreased by 0.36 mm (SD 0.26 mm; 95% CI, 0.17 to 0.55 mm; $P < .001$) for the right limbs and 0.35 mm (SD 0.19 mm; 95% CI, 0.21 to 0.49 mm; $P < .001$) for the left limbs. Cardiac pulsatility–induced changes in curvature, limb length, and inter-ring distance were negligible (2%, 0.3% and 0.3%, respectively). Changes in the geometry of the Anaconda endograft limbs after endovascular aortic aneurysm repair were observed during a 2-year follow-up manifest as an increase in curvature, shortening of the stent-graft limbs, and a corresponding decrease in inter-ring distance. These stent-graft conformational changes could result in inward folding of the graft fabric, which may relate to the emergence of limb

R. H. Geelkerken is a consultant for Terumo Aortic.

Part of this work was presented at the ESCVS International Congress May 22–25, 2019, Groningen, The Netherlands.

*Corresponding author.
E-mail address: j.a.simmering@utwente.nl (J.A. Simmering).

https://doi.org/10.1053/j.semvascsurg.2019.11.001

occlusion. Further investigation of these metrics in a larger cohort involving patients with and without occlusions may allow determination of their predictive value.

1. Introduction

Progress in endovascular aortic aneurysm repair (EVAR) has been made by advances in endograft design and image-guided endovascular techniques. However, compared to open surgery, the benefits of this less-invasive procedure [1,2] are challenged by a considerable reintervention rate up to 20% in the first 5 years after EVAR due to complications including endoleak, device migration, and limb occlusion [2–4]. Since its introduction in 1998, the Anaconda endograft (Terumo Aortic, Inchinnan, Scotland, UK) has evolved to a third-generation device (One-Lok) with an independent nitinol stent-ring design to optimize device conformability and compatibility with tortuous anatomy. The Anaconda design has demonstrated durable aneurysm exclusion in daily practice [5–7] with a low reported number of type I endoleaks (3.5% *vs.* 4.2% to 8.5% for other endografts), type III endoleaks (0.6% *vs.* 0% to 1.5% for other endografts), and endograft migration (0.6% *vs.* 0% to 0.9% for other endografts) [4]. Still, a recent single-center study involving 110 elective patients with a One-Lok Anaconda device reported an overall limb occlusion rate of 6.4% after a mean follow-up of 47 months, while the incidence of iliac limb occlusion was estimated at 5.6% in a recent meta-regression analysis involving 5,454 patients [8]. These results indicate that further efforts may be needed to optimize the next generation of Anaconda limbs in order to reduce the incidence of limb occlusion. Previous studies have identified predisposing factors that increase the risk of occlusion, including significant angulation and calcification of the iliac arteries, excessive limb oversizing, small distal limb diameter, small external iliac artery diameter extension of the endograft limb into the external iliac artery, and kinking [7,9–13]. Albeit useful to help define specific treatment strategies, these factors do not help to select patients at risk during follow-up, as they do not provide insight into the ongoing interaction between the endograft configuration and the patient's anatomy. Moreover, detailed information about changes in limb geometry several months to years after EVAR is lacking in the literature. Understanding these changes may help to identify potential predictors of limb occlusion and additionally to improve endograft design. We hypothesize that shrinkage of the aneurysm sac may result in changes in the initial configuration, including changes in limb length and limb angulation. Due to the independent stent-ring configuration of the Anaconda limbs, these changes may lead to inward folding of the endograft fabric, which may contribute to the emergence of limb embolization or thrombosis by inducing regions with static, recirculating, and turbulent flow patterns [11,14]. Additionally, pulsatile blood flow may induce cyclic geometric changes in limb configuration, potentially affecting flow patterns. The aim of this work was to provide detailed information about geometric changes of Anaconda endograft limbs during follow-up, as well as during the cardiac cycle.

2. Methods

This study used postoperative electrocardiogram (ECG)-gated computed tomography (CT) scans of 15 patients with asymptomatic infrarenal abdominal aortic aneurysm (AAA) (mean age 72.8 ± 3.7 years; 14 men) who underwent elective EVAR with an Anaconda One-Lok endograft between April 2014 and May 2015. These patients were prospectively enrolled in an observational single-center cohort study (Longitudinal Study of Pulsatility and Expansion in Aortic Stent-grafts [LSPEAS], Trialregister.nl identifier: NTR4276) and were followed for 24 months after EVAR by ECG-gated CT scans according to a standardized protocol: before discharge and after 1, 6, 12, and 24 months follow-up. The study design, patient sample, and image acquisition protocol have been reported in detail previously [15]. Additional patient characteristics related to the iliac anatomy and implanted endograft limbs are presented in Table 1. The CT scans were acquired during a single breath-hold and were reconstructed into 10 phases to cover the cardiac cycle with a slice thickness of 1 mm. The CT scans were performed without contrast administration to preclude nephrotoxic effects. Two of the 15 patients did not undergo the 24-months scan (non-AAA–related death and voluntary withdrawal).

2.1. *The Anaconda Device*

The Anaconda endograft design, characteristics, and implant technique have been described in detail previously [5,16,17]. Here, we briefly describe the Anaconda limb characteristics. The limbs consist of multiple independent nitinol stent rings that are sewn onto the woven polyester graft fabric, providing flexibility in tortuous iliac arteries [16]. The One-Lok Anaconda bifurcate body has a standardized iliac gate diameter of 10.5 mm to facilitate the standard 12-mm proximal limb diameter. To improve body–limb combinations for patient-specific sizing, the distal outflow configuration can be tapered, straight, or flared, with stent-ring diameters ranging from 10 to 23 mm. The distance between the 12-mm stent rings is 5.5 mm. For a 10-mm tapered end, the inter-ring distance is 4.5 mm. For a flared end, the inter-ring distance increases with increasing stent-ring diameter up to 10 mm for a 23-mm flared limb.

2.2. *ECG-gated CT image processing and analysis*

The ECG-gated CT scans were processed using a previously developed algorithm that uses image registration to estimate motion and image segmentation to model geometry of the endograft's stent frame [18–20]. The purpose of the image registration was two-fold: to obtain a deformation (i.e., vector) field for each reconstructed phase in the cardiac cycle in order to obtain a phase-averaged 3-dimensional (3D) volume for image segmentation, and to evaluate motion and deformation

Table 1 – Patient iliac anatomy characteristics.[a]

Patient IDs	01	02	03	05	08	09	11	15	17	18	19	20	21	22	25	Mean ± SD
R-IA length, mm	40	50	60	70	80	60	50	60	80	75	55	80	55	60	73	65 ± 11,1
L-IA length, mm	45	70	55	70	50	50	60	40	90	95	70	90	70	77	55	66 ± 17,1
R-IA diameter landing zone, mm	13	9	11	10	12	15	20	8	14	13	19	12	14	23	11	14 ± 4,2
L-IA diameter landing zone, mm	8	8	11	9	9	12	12	13	11	15	16	12	9	23	12	12 ± 3,9
R landing zone in CIA	Yes	Yes	Yes	Yes	Yes	Yes	Yes	No	No	Yes	Yes	Yes	Yes	Yes	Yes	—
L landing zone in CIA	No	Yes	Yes	Yes	Yes	Yes	No	Yes	Yes	Yes	Yes	Yes	No	Yes	Yes	—
R-IA angulation (°)	112	40	37	35	97	78	52	37	41	28	44	84	89	101	97	69 ± 33.5
L-IA angulation (°)	111	26	42	48	104	6	43	58	65	81	117	101	100	136	52	77 ± 44.3
R-IA calcification, %	—	40	—	50	10	20	20	30	20	10	10	0	30	80	20	26 ± 21,0
L-IA calcification, %	20	25	—	50	20	20	20	30	60	10	20	0	30	80	20	29 ± 21,0
R-IA thrombus, %	70	0	0	0	0	0	0	0	0	0	0	0	0	0	0	5 ± 18,1
L-IA thrombus, %	80	0	0	0	0	0	0	0	0	0	0	0	0	0	0	5 ± 20,7
R limb oversizing, %	15	11	9	20	8	13	15	25	21	15	11	25	21	0	9	15 ± 7.9
L limb oversizing, %	25	25	9	33	33	25	0	15	18	13	19	25	11	0	25	19 ± 10.4
R limb length, mm	130	130	140	140	130	110	130	140	130	130	130	130	130	100	140	129 ± 11.0
Extension length, mm	—	80	—	—	—	80	—	80	—	—	—	—	120	110	—	94 ± 19.5
R distal limb diameter, mm	15	10	12	12	13	17	23	10	17	15	21	15	17	23	12	15 ± 4.3
L limb length, mm	130	130	140	140	120	130	140	130	130	130	130	130	140	100	80	127 ± 16.3
Extension length, mm	80	80	—	—	—	—	80	85	—	—	—	—	130	130	80	95 ± 24
Bridge length, mm	—	—	—	—	—	—	—	—	—	—	—	—	80	—	—	80
L distal limb diameter, mm	10	10	12	12	12	15	12	15	13	17	19	15	10	23	15	14 ± 3.6

Abbreviations: CIA, common iliac artery; IA, iliac artery; ID, study identification number; L, left; R, right; SD, standard deviation.
[a]According to EUROSTAR [30].

of the limb geometry during the cardiac cycle. By using deformable registration, the phase-averaged 3D volumes representing mid–cardiac cycle were compensated for motion artefacts to allow for assessment of limb deformation. The image-processing steps have been detailed previously [20]. The algorithm was further refined to evaluate curvature and length of the limbs by obtaining center lumen lines (CLLs) (Fig. 1A). A threshold segmentation (>600 Hounsfield units) was performed to obtain a set of points that described the stent frame. The CLLs were extracted by calculating the path through the center of the respective set of points of the stent frame by maximizing the distance to these points. The start of the CLL was defined at the level of the most proximal stent ring in the limb; the end at the level of the most distal stent ring. The CLLs comprise a set of consecutive points with a set distance of 1 mm. All CLLs were inspected visually. To quantify distances between the stent rings of the limbs (eg, perceived increased risk of limb occlusion related to inward folding of graft fabric), we created 3D geometric models of each stent ring. To obtain individual stent-ring models, seed points for initialization were manually selected per stent ring, after which the stent-ring models were obtained automatically [19]. To evaluate cardiac-induced changes of the metrics, the CLLs and stent-ring models that were generated in the phase-averaged 3D volumes were transformed to the 10 phases of a cardiac cycle by backward mapping of the deformation fields. Applying this image registration algorithm instead of repeating the measurements in the different phases of the cardiac cycle is time-efficient and avoids inconsistencies between the models and CLLs in the different phases, which can drastically reduce the accuracy of the measurements.

2.3. *Curvature*

Curvature was defined as the inverse of the radius of the spherical shape that best approximates the curve at each point along the CLL, expressed in m^{-1} (Fig. 1). Mathematically, curvature was calculated for a parametrically defined 3D curve (equation 1):

$$\kappa = \frac{\sqrt{(z''y' - y''z')^2 + (x''z' - z''x')^2 + (y''x' - x''y')^2}}{(x'^2 + y'^2 + z'^2)^{3/2}}, \quad (1)$$

where $x(n)$, $y(n)$, and $z(n)$ are the Cartesian coordinates in 3 dimensions for the number of points n along the CLL, $'$ is the first derivative and $''$ is the second derivative. The curvature calculation was implemented in Matlab 2018a (The Mathworks, Natick, MA) and was validated using a helix-shaped phantom that was designed to validate curvature calculations [21]. Larger curvature values indicate a stronger limb angulation, that is, larger limb curvature. Change in mean and maximum curvature during follow-up was assessed for each limb by comparing these metrics at mid–cardiac cycle. Furthermore, mean and maximal cardiac pulsatility–induced changes in curvature were evaluated in each scan. Maximal change in curvature indicated the largest change in curvature at a particular CLL point and mean change indicates the average change of all CLL points.

2.4. *Limb length*

The length of the endograft limbs was assessed as the length of the CLLs in millimeters. The change in limb length was evaluated over time at mid-cardiac cycle and in each scan

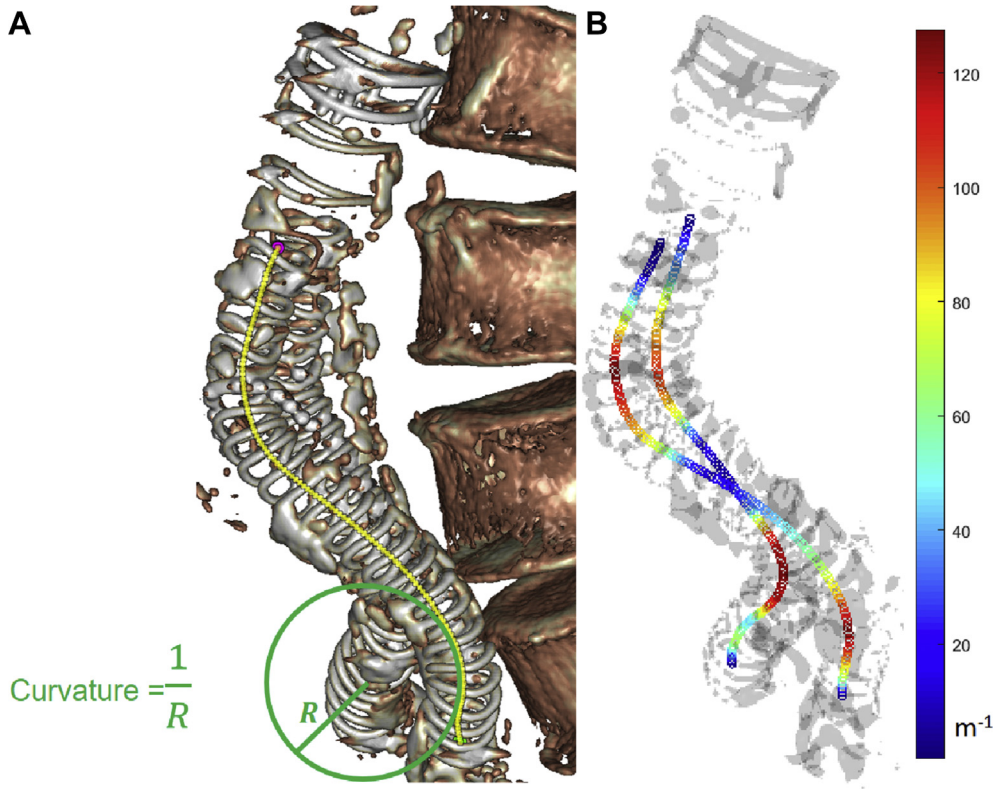

Fig. 1 – An example of the assessment of curvature over the center lumen line (CLL), illustrating (A) the calculation of curvature over the CLL along with (B) the color-coded curvature that was calculated for each point of the CLL of both limbs (blue represents low curvature, i.e., straight; red represents high curvature, i.e., angulated). R, radius of curvature.

during the cardiac cycle by comparing the limb length in each phase of the cardiac cycle.

2.5. *Distances between stent rings*

Distances were calculated between successive stent rings, that is, inter-ring distances. For each pair of successive stent rings, the shortest distance from each point on the most cranial stent ring to a point on the successive stent ring was automatically obtained. These distances were used to calculate mean and minimal inter-ring distance for each ring pair (expressed in millimeters; Fig. 2). For each limb, the mean and minimal inter-ring distance were calculated by taking the average of the mean and minimal inter-ring distances of all ring pairs. Change in mean and minimal inter-ring distance during follow-up was assessed by comparing these metrics at mid–cardiac cycle. Again, cardiac-induced changes in distance were evaluated in each scan.

2.6. *Statistical analysis*

Normality of the data was checked by histograms. The data were found to be normally distributed and was displayed as mean values followed by the standard deviation (SD) and the 95% confidence interval (CI). Mixed-model repeated-measures analysis was performed to assess changes in curvature, limb length, and inter-ring distances during follow-up. A fixed-effects model was used to evaluate differences in change between the right and left limb at different time points relative to discharge with the assumption that changes in the right and left limbs were unrelated. The optimal covariance type was selected per analysis based on Akaike's Information Criterion. A post-hoc Sidak correction was used to correct for multiple comparisons. The 2-tailed Pearson's correlation coefficient (PCC) was used to investigate the relationship between different metrics. For all analyses, a significance level of $P < .05$ was assumed statistically significant. Statistical analyses were performed using SPSS Statistics, version 25.0 (IBM Corp, Armonk, NY).

3. Results

Table 2 presents geometric changes in curvature, limb length, and inter-ring distance in the Anaconda endograft left and right limbs through the 24-month follow-up period.

3.1. *Curvature*

Figure 3 presents the change in mean and maximal curvature from discharge to 24 months after EVAR. For all patients, mean and maximal curvature of both limbs had increased over time. From discharge to 24 months, mean curvature increased significantly by 9.6 m^{-1} (SD 11.1 m^{-1}; 95% CI, 3.4 to 15.8 m^{-1}; $P = .002$) for the right limbs and by 6.1 m^{-1} (SD 9.4 m^{-1}; 95% CI, 0.8 to 11.5 m^{-1}; $P = .21$) for the left limbs. Maximal

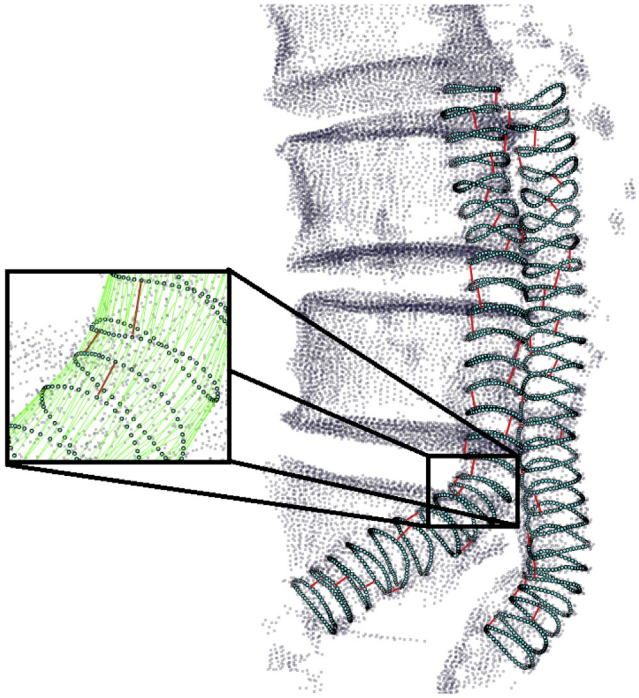

Fig. 2 – Example of the assessment of inter-ring distances between successive stent-rings. The 3-dimensional geometric models of the individual stent rings are shown for which distances between the points on the successive stent rings were automatically calculated (green lines in the box magnification). The minimal distance between each pair of stent rings is indicated with red lines.

curvature increased significantly for the right limbs by 28.3 m^{-1} (SD 32.2 m^{-1}; 95% CI, 3.0 to 53.6 m^{-1}; $P = .025$), but not for the left limbs (7.7 m^{-1}; SD 22.4 m^{-1}; 95% CI, −4.5 to 20.0 m^{-1}; $P = .330$). On average, this is an increase of 56% (SD 46%) of the mean curvature measured at discharge and an increase of 52% (SD 73%) of the maximal curvature. The change in curvature from discharge to 24 months of the left and right limbs was not significantly different for mean ($P = .294$) or maximal curvature ($P = .060$).

The location of maximal curvature on the CLL, measured from the proximal end, moved cranially during the 24-month follow-up period for both the right and the left limbs (right: 25.0 mm, SD 40.5 mm; 95% CI, −1.8 to 51.8 mm; $P = .072$; left: 33.9 mm, SD 31.9 mm; 95% CI, 9.3 to 58.5 mm; $P = .005$). There was no significant difference between both limbs ($P = .573$), resulting in an overall shifting from 103.9 mm (SD 43.8 mm; 95% CI, 87.1 to 118.8 mm) to 66.9 mm (SD 39.7 mm; 95% CI, 57.1 to 89.6 mm) from the proximal end of the CLL by a mean change of 29.6 mm (SD 35.0 mm; 95% CI, 11.5 to 47.7 mm; $P = .001$).

During the cardiac cycle, the mean and maximal change in curvature ranged from 0.0292 to 1.497 m^{-1} and from 0.493 to 4.167 m^{-1}, respectively. These changes are, on average, 1.2% and 2.2% of the smallest mean and maximal curvature values. respectively, during the cardiac cycle. An example of cardiac pulsatility–induced changes in CLL geometry and curvature is shown in Figure 4A and B. The changes in mean and maximal curvature during the cardiac cycle did not significantly differ between the right and left limbs ($P > .422$) or between time points during follow-up ($P > .096$).

3.2. *Limb length*

The length of the limbs decreased significantly from discharge to 24 months by 9.6 mm (SD 6.8 mm; 95% CI, 6.0 to 13.2 mm; $P < .001$). Right limbs decreased in length by 9.5 mm (SD 7.6 mm; 95% CI, 3.5 to 15.6 mm; $P = .002$) and left limbs by 10.1 mm (SD 5.1 mm; 95% CI, 5.9 to 14.2 mm; $P < .001$) (Fig. 5). On average, this is a decrease of 7.6% (SD 5.0%) of the length at discharge. No significant difference in change in limb length was observed between right and left limbs ($P = .877$).

Change in limb length during cardiac cycle ranged from 0.09 to 1.22 mm and was not statistically different between the right and left limbs ($P = .894$). On average, the cardiac pulsatility–induced changes were 0.3% of the smallest limb length during the cardiac cycle. During follow-up, these changes were statistically different between discharge and 1 month only (−0.100 mm *vs.* −0.006 mm; $P = .033$).

3.3. *Distances between rings*

A decrease was observed in the mean inter-ring distance from discharge to 24 months (all limbs: 0.17 mm, SD 0.14 mm; 95% CI, 0.10 to 0.25 mm; $P < .001$; right: 0.17 mm, SD 0.17 mm; 95% CI, −0.04 to 0.29 mm; $P = .004$; left: 0.18 mm, SD 0.14 mm; 95% CI, 0.11 to 0.25 mm; $P < .001$; Fig. 6). Similarly, the minimal inter-ring distance decreased by 0.36 mm (SD 0.24 mm; 95% CI, 0.24 to 0.48 mm; $P < .001$) for all limbs, 0.36 mm (SD 0.26 mm; 95% CI, 0.17 to 0.55 mm; $P < .001$) for the right limbs, and 0.35 mm (SD 0.19 mm; 95% CI, 0.21 to 0.49 mm; $P < .001$) for the left limbs (Fig. 6). These differences between the right and left limbs were not statistically significant ($P > .763$).

Cardiac pulsatility–induced changes in mean and minimal inter-ring distances ranged from 0.004 mm to 0.030 mm and from 0.004 mm to 0.021 mm, respectively. This is, on average, 0.3% of the smallest minimal inter-ring distances during the cardiac cycle. Figure 4C shows an example of cardiac-induced changes in minimal inter-ring distances. During follow-up, these changes did not differ between time points ($P > .082$) except for minimal inter-ring distance between discharge and 1-month follow-up (0.010 mm, SD 0.004 mm *vs.* 0.008, SD 0.003 mm; $P = .038$).

3.4. *Correlations between metrics*

The change in mean curvature during the 24-month follow-up period correlated with the change in minimal inter-ring distance (PCC = −0.63; $P = .001$) and the change in limb length (PCC = −0.47; $P = .016$). Additionally, the change in limb length correlated positively with the change in minimal inter-ring distance during 24-month follow-up (PCC = 0.86; $P < .001$). Furthermore, the 24-month change in aneurysm sac diameter significantly correlated with the change in limb length (PCC = 0.43; $P = .028$) and minimal inter-ring distances (PCC = 0.41; $P = .039$), but not with the change in mean curvature (PCC = −0.31; $P = .121$).

Table 2 – Evolution of geometric changes in the Anaconda endograft limbs through the 24-month follow-up period.

Variable	Discharge (n = 15)	1 month (n = 15)	6 months (n = 15)	12 months (n = 15)	24 months (n = 13)
Curvature, m^{-1}, mean ± SD (95% CI)	18.88 ± 4.43 (17.23 to 20.54)	19.35 ± 5.06 (17.45 to 21.24)	21.89 ± 6.58 (19.43 to 24.35)	24.85 ± 7.17 (22.17 to 27.53)	27.02 ± 8.71 (23.76 to 30.28)
Curvature change,[a] m^{-1}, mean ± SD (95% CI)	—	0.46 ± 1.89 (–0.45 to 1.38)	3.00 ± 4.00 (1.06 to 4.95)	5.96 ± 5.35 (–3.37 to 8.56)	8.14 ± 7.18 (4.38 to 11.90)
P value	—	.568	.001	<.001	<.001
Maximal curvature, m^{-1}, mean ± SD (95% CI)	57.69 ± 25.22 (48.24 to 67.14)	57.54 ± 25.72 (47.87 to 67.20)	58.80 ± 23.78 (49.76 to 67.84)	67.06 ± 26.71 (56.98 to 77.13)	74.45 ± 29.56 (64.69 to 86.44)
Maximal curvature change,[a] m^{-1}, mean ± SD (95% CI)	—	–0.15 ± 8.95 (–4.50 to 4.20)	1.11 ± 16.05 (–6.69 to 8.91)	9.37 ± 22.69 (–1.66 to 20.39)	17.88 ± 26.49 (4.04 to 31.72)
P value	—	1.000	.993	.121	.007
Maximal curvature location, mm, mean ± SD (95% CI)	103.9 ± 43.8 (87.1 to 118.8)	101.5 ± 46.7 (85.7 to 117.4)	96.4 ± 42.7 (80.52 to 112.2)	85.2 ± 48.2 (69.4 to 101.0)	66.9 ± 39.7 (57.1 to 89.6)
Maximal curvature location change,[a] mm, mean ± SD (95% CI)	—	–1.4 ± 28.57 (–14.5 to 11.7)	–6.6 ± 32.1 (–21.4 to 8.3)	–17.7 ± 36.2 (–34.6 to –0.7)	–29.6 ± 35.0 (–47.7 to –11.5)
P value	—	.998	.711	.038	.001
Limb length, mm, mean ± SD (95% CI)	147.5 ± 30.5 (136.0 to 159.0)	145.7 ± 30.0 (134.4 to 157.0)	142.1 ± 30.3 (130.7 to 153.6)	140.5 ± 30.3 (129.1 to 151.9)	132.9 ± 30.3 (125.7 to 150.2)
Limb length change,[a] mm, mean ± SD (95% CI)	—	–1.8 ± 1.5 (–2.6 to –1.1)	–5.4 ± 3.6 (–7.1 to –3.6)	–7.1 ± 4.7 (–9.3 to –4.8)	–9.6 ± 6.8 (–13.2 to –6.0)
P value	—	<.001	<.001	<.001	<.001
Mean inter-ring distance, mm, mean ± SD (95% CI)	4.67 ± 0.33 (4.54 to 4.80)	4.65 ± 0.35 (4.52 to 4.78)	4.61 ± 0.34 (4.48 to 4.74)	4.56 ± 0.35 (4.43 to 4.69)	4.49 ± 0.39 (4.36 to 4.63)
Mean inter-ring distance change,[a] mm, mean ± SD (95% CI)	—	–0.02 ± 1.48 (–0.09 to 0.05)	–0.06 ± 1.48 (–0.13 to 0.01)	–0.11 ± 1.48 (–0.18 to –0.05)	–0.17 ± 1.43 (–0.25 to –0.10)
P value	—	.956	.089	<.001	<.001
Minimal inter-ring distance, mm, mean ± SD (95% CI)	3.71 ± 0.42 (3.55 to 3.86)	3.72 ± 0.43 (3.56 to 3.87)	3.64 ± 0.37 (3.49 to 3.79)	3.55 ± 0.37 (3.40 to 3.70)	3.39 ± 0.42 (3.20 to 3.50)
Minimal inter-ring distance change,[a] mm, mean ± SD (95% CI)	—	0.01 ± 0.46 (–0.11 to 0.12)	–0.07 ± 0.46 (–0.18 to 0.05)	–0.16 ± 0.46 (–0.27 to –0.04)	–0.36 ± 0.40 (–0.48 to –0.24)
P value	—	.999	.485	.003	<.001

Abbreviations: CI, confidence interval; SD, standard deviation.
[a]Change indicates the difference to discharge.

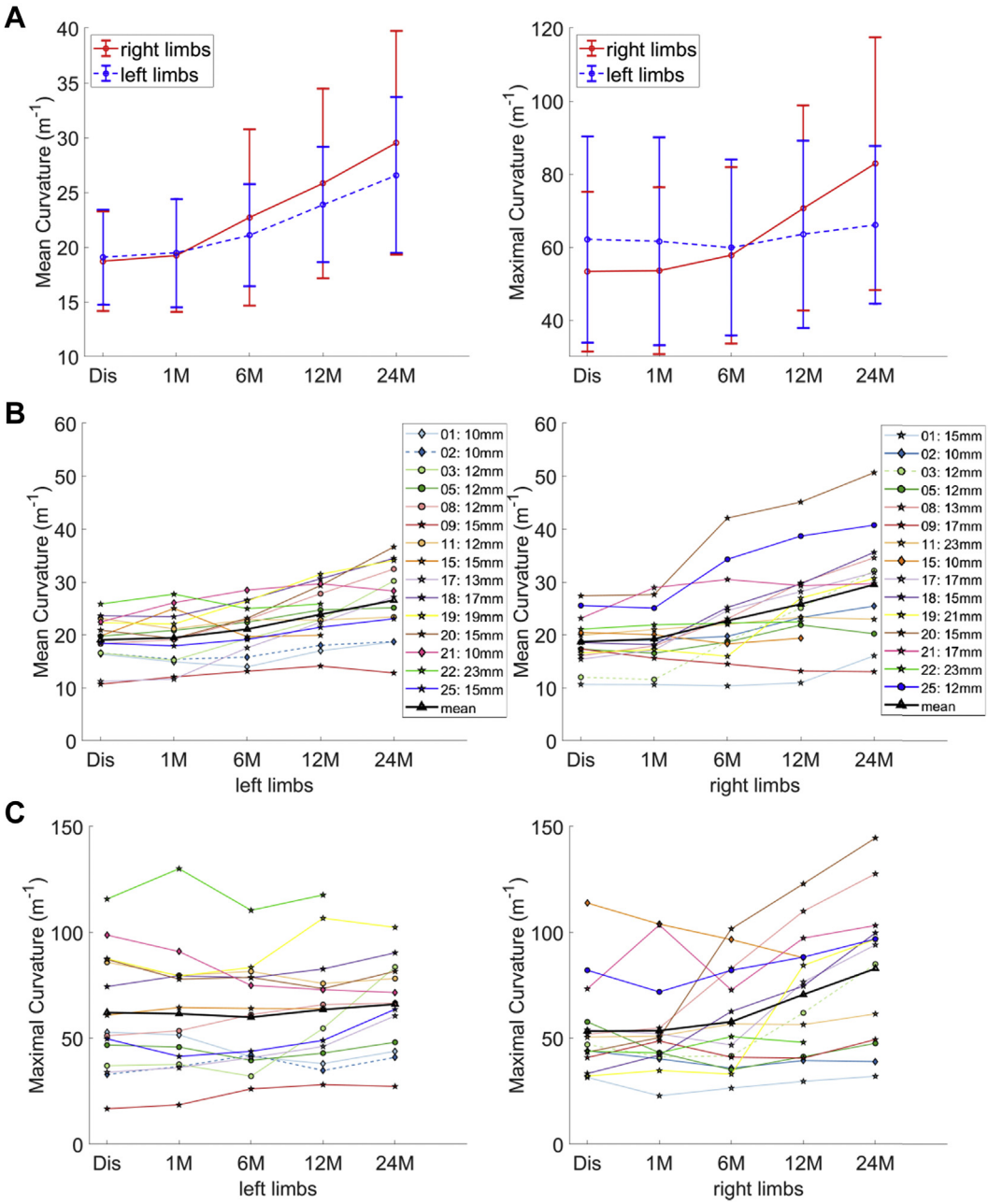

Fig. 3 – Evolution of mean and maximal curvature of the left and right limbs of the Anaconda endograft from discharge to 24 months endovascular aortic aneurysm repair (EVAR). The mean (dot) and standard deviation (whiskers) are displayed (A), as well as the values of the mean (B) and maximal (C) curvature for each individual patient. The distal diameters of the limbs are shown for each patient in the legend, where 3 types of markers are indicated: tapered (◊), straight (o), and flared (★). Dis, discharge; M, months after EVAR.

3.5. *Patients with limb occlusion*

In 2 of the 15 patients, unilateral limb occlusions were observed 27 months after EVAR (patient 2, left limb; patient 3, right limb). The limb occlusions were treated by endovascular recanalization (thrombectomy) and endolining (10-mm Advanta V12 balloon-expandable covered stents; Maquet Getinge Group, Hudson, NH). Patency remained to date, 3 years after reintervention.

For these patients, the metrics considered here (curvature, limb length, and inter-ring distance) are shown as dotted lines in Figures 3, 5, and 6.

4. Discussion

The present study evaluated, in detail, geometrical changes in Anaconda endograft limbs over time and during cardiac cycle

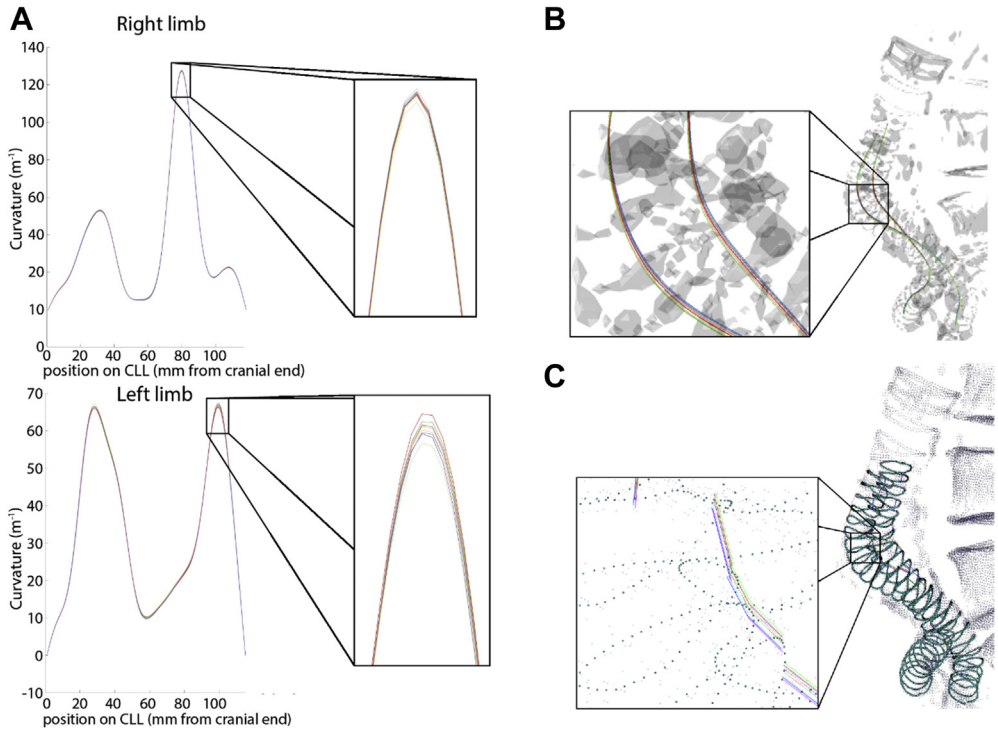

Fig. 4 – An example of cardiac pulsatility–induced changes in limb geometry in 1 patient. (A) Curvature along the center lumen line (CLL) for the 10 different phases in a cardiac cycle; points on the CLL are in consecutive order, starting at the proximal point of the CLL. (B) Three-dimensional view of the CLLs in each phase in a cardiac cycle. (C) Three-dimensional view of the stent-ring models at mid–cardiac cycle with the minimal inter-ring distances shown for each phase in a cardiac cycle. Each line represents 1 cardiac phase.

by quantifying curvature of the limbs, limb length, and distances between successive stent rings in the limbs (inter-ring distance). During 24-month follow-up, curvature increased and limb length and inter-ring distances decreased. Change in minimal inter-ring distance correlated with the change in mean curvature, limb length, and AAA sac diameter, which suggests that these metrics may be related to the emergence of limb occlusion by inward folding of the graft fabric as the inter-ring distance decreases. Another relevant finding of this study is that geometry changes per heartbeat in curvature, limb length, and inter-ring distance were negligible (2%, 0.3% and 0.3%, respectively).

Recently, Rödel et al [7] observed a 6.4% limb occlusion rate in the third-generation device compared to a 13.1% limb occlusion rate in the second-generation device at a mean follow-up of 47 months. This suggests that there is room for improvement, as the average rate of limb occlusion was reported 5.6% [8]. Iliac limb angulation of $\geq$60 degrees, distal limb diameter of $\leq$13 mm, iliac calcification, and extension of the limb (into the external iliac artery) are known predisposing factors for limb occlusion [7,9,10,12,13]. However, limb occlusion also emerges in patients without these predisposing factors, and occlusions may be related to post-EVAR changes in limb configuration, as observed in the present study. Shrinkage of the AAA sac, which occurs also longitudinally [22], seems to cause a shortening of the limb length and a decrease in inter-ring distance. Shortening of the limbs may also form regions with increased curvature, which could explain the observation that the location of maximum curvature shifts cranially into the AAA sac. Inward folding of the graft fabric and increased angulation can result in regions of fluid stasis and high shear stress, which are known to increase the platelet activation potential and thus increase the risk of thrombus formation [23].

The limited changes during the cardiac cycle are not an unexpected finding because the difference between the arterial pressure inside the stent graft and the AAA sac pressure outside the stent graft is small throughout the cardiac cycle due to a lack of pulse wave in the sac that even decreases further over time [24]. In addition, aortic distension after EVAR at the level of maximum AAA diameter was previously observed to be small per cardiac cycle [25,26], as well as variations in stress and strain in limbs of various EVAR endografts between systole and diastole [27]. Still, the observed cardiac pulsatility–induced changes in curvature are slightly higher than the curvature change reported by Itoga et al [28] for the Nellix device (Endologix Inc, Irvine, CA). This is probably due to the difference in stent-graft design, where the Nellix device uses stiff balloon-expandable stent-grafts and the Anaconda device has flexible self-expanding stent-graft limbs with no lower column strength.

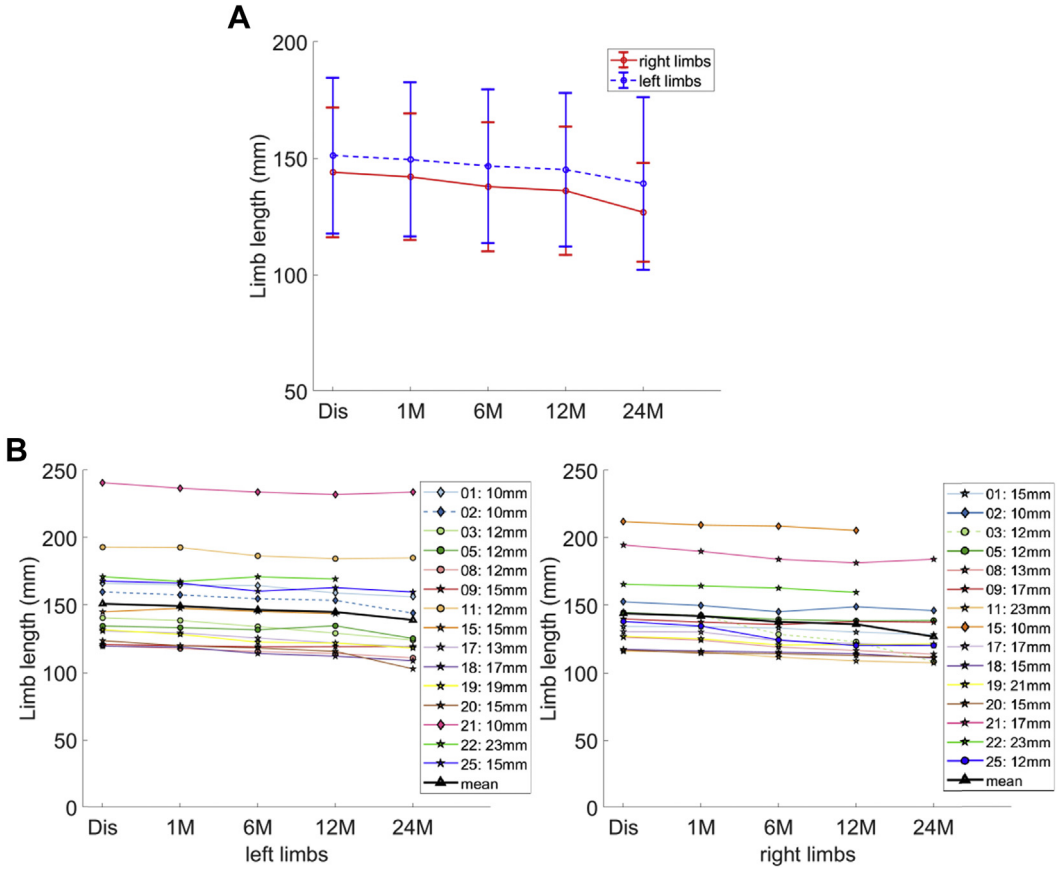

Fig. 5 – Evolution in limb length of the left and right limbs of the Anaconda endograft from discharge to 24 months after endovascular aortic aneurysm repair (EVAR). The mean (dot) and standard deviation (whiskers) are displayed (A) as well as the limb length for each individual patient. The distal diameters of the limbs are shown for each patient in the legend, where 3 types of markers are indicated: tapered (◊), straight (o), and flared (★). Dis, discharge; M, months after EVAR.

Notably, 2 of the 15 patients developed limb occlusion 27 months after EVAR. We observed several interesting differences compared to the other patients. In 1 patient (patient 3), the occluded limb showed an increase in curvature far above average and the largest decrease in limb length and inter-ring distance. The other patient (patient 2) showed an average increase in curvature, but presented a small inter-ring distance from discharge on, with an apparent decrease in limb length and mean inter-ring distance from 12 to 24 months. Minimal inter-ring distance decrease was even perceivable from 6 months on. In both patients, the inter-ring distances of the occluded limb were the smallest of all limbs at 24 months follow-up, that is, shortly before they were diagnosed with limb occlusion. In addition, these 2 patients have relatively small distal limb diameters ($\leq$12 mm), for which the incidence of limb occlusion appears to be higher [7]. While other limbs also showed small inter-ring distances similar to the occluded limbs, in those cases the inter-ring distances did not decrease, except in 1 patient (patient 1, left limb) who, based on these observations, might be at risk to develop limb occlusion. However, the relation of the geometric changes considered in the present study, complementary to known predisposing factors, should be further investigated in a larger cohort comprising patients that have and have not presented with limb occlusion.

Finally, it should be noted that the initial mean inter-ring distance was always below the fabricated 5.5-mm straight limb inter-ring distance. This implies that the limbs may not have been deployed to their full length, possibly due to overestimation of the required limb length, which is not uncommon, especially in angulated anatomies [29]. Also, extension of the limbs (12 of the 30 limbs were extended) may lead to introduction of limbs that exceed the length of the iliac anatomy and, consequently, upward pushing of the limbs during intervention, inducing smaller inter-ring distances. Therefore, we recommend measuring the length of device limb required 3-dimensionally and to stretch out the limbs during intervention in order to prevent inward folding of graft fabric due to small inter-ring distances.

The present study involved a relatively small patient cohort, which is an outcome analysis limitation. This was, in part, related to our local regular EVAR follow-up protocol that dictates the use of duplex ultrasound instead of CT

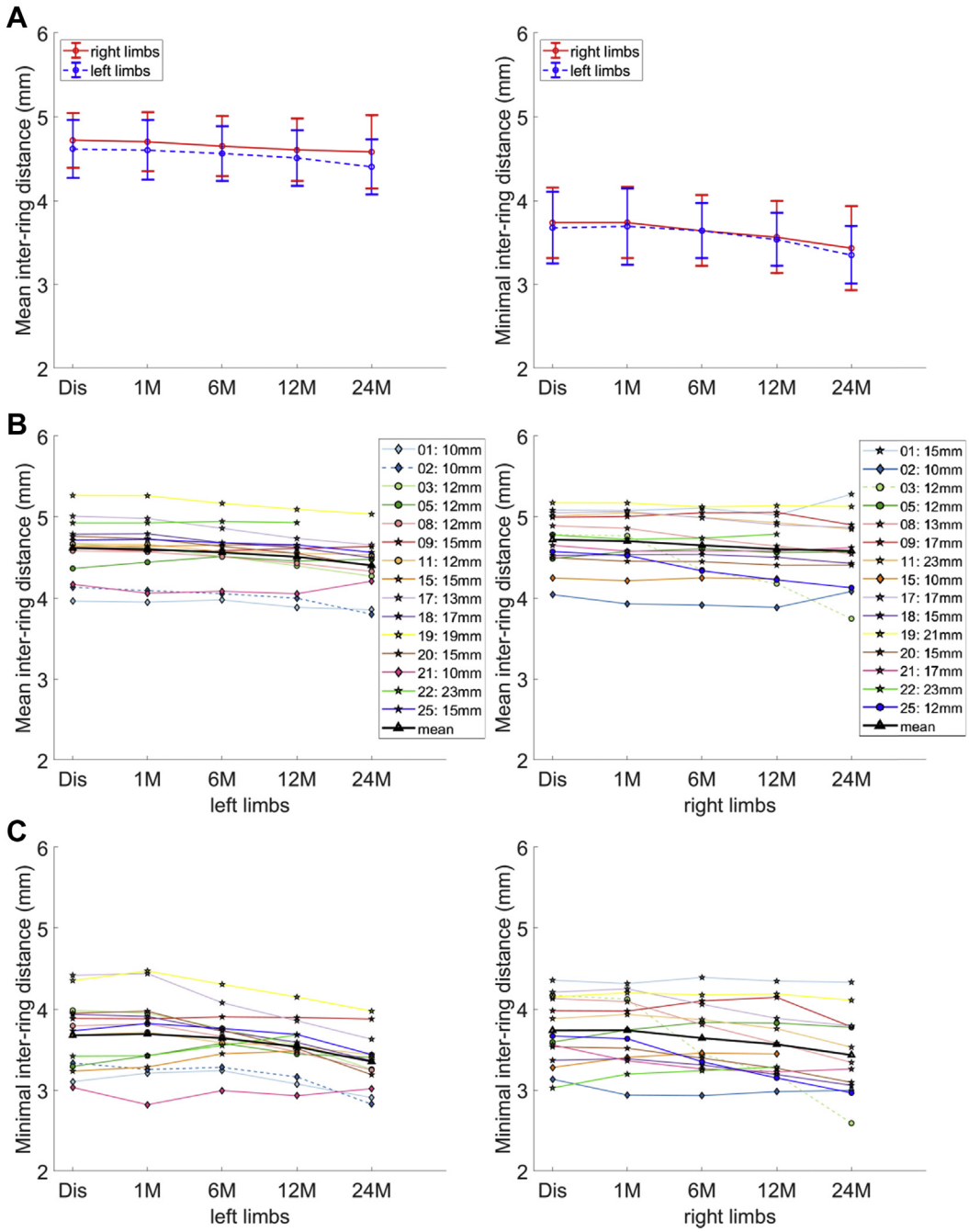

Fig. 6 – Evolution of mean and minimal inter-ring distance of the left and right limbs of the Anaconda endograft from discharge to 24 months after endovascular aortic aneurysm repair (EVAR). The mean (dot) and standard deviation (whiskers) are displayed (A), as well as the values of the mean (B) and minimal (C) inter-ring distances for each individual patient. The distal diameters of the limbs are shown for each patient in the legend, where 3 types of markers are indicated: tapered (◊), straight (o), and flared (★). Dis, discharge; M, months after EVAR.

examinations. Nevertheless, the ECG-gated CT scans, prospective study design with close follow-up, and meticulous processing methods allowed for in-depth evaluation of both geometry changes during follow-up and changes due to pulsatile blood flow, which cannot be achieved in static CT scans. Furthermore, it should be noted that the small cardiac pulsatility–induced changes approached the experimentally derived detection limit of 0.3 mm [20]. Finally, because modeling the individual stent rings is currently time-consuming, the methodology should be further optimized in order to use the measurement of inter-ring distances in clinical practice.

5. Conclusions

The findings of this study indicate the geometry of the Anaconda stent-graft limbs changes over time, as evidenced by an increase in curvature, shortening of the limbs, and a corresponding decrease in distance between successive stent-rings. In 2 of the 15 patients, stent-graft limb occlusion occurred and may be related to device conformational changes, a result of the inward folding of the graft fabric. The CT scan metrics confirmed in this study may provide an etiology to occurrence of limb occlusion with the Anaconda stent graft. Our findings support the study in a larger patient cohort with and without limb occlusions to verify the relationship of conformational change and stent-graft thrombosis.

Acknowledgements

The authors thank Prof. Dr. J. A. M. van der Palen (clinical epidemiologist, Medisch Spectrum Twente/ University of Twente) and Dr. M. Haalboom (clinical epidemiologist, Medisch Spectrum Twente/postdoctoral researcher, University of Twente) for their support with the statistical analyses. The authors also thank S. Cnossen, MSc, for his contribution during his Technical Medicine internship.

This work was supported in part by an unrestricted grant from Vascutek Terumo, trading as Terumo Aortic, and in part by the PPP Allowance made available by Health-Holland, Top Sector Life Sciences & Health, to stimulate public-private partnerships, for which the authors are greatful.

REFERENCES

[1] Prinssen M, Verhoeven ELG, Buth J, et al. A randomized trial comparing conventional and endovascular repair of abdominal aortic aneurysms. N Engl J Med 2004;351:1607–18.
[2] Patel R, Sweeting MJ, Powell JT, et al. Endovascular versus open repair of abdominal aortic aneurysm in 15-years' follow-up of the UK Endovascular Aneurysm Repair Trial 1 (EVAR trial 1): a randomised controlled trial. Lancet 2016;388:2366–74.
[3] Nordon IM, Karthikesalingam A, Hinchliffe RJ, et al. Secondary interventions following endovascular aneurysm repair (EVAR) and the enduring value of graft surveillance. Eur J Vasc Endovasc Surg 2010;39:547–54.
[4] Jonker LT, de Niet A, Reijnen MMPJ, et al. Mid- and long-term outcome of currently available endografts for the treatment of infrarenal abdominal aortic aneurysm. Surg Technol Int 2018;33:239–50.
[5] Rödel SGJ, Zeebregts CJ, Huisman AB, et al. Results of the Anaconda endovascular graft in abdominal aortic aneurysm with a severe angulated infrarenal neck. J Vasc Surg 2014;59:1495–1501.e1.
[6] Freyrie A, Gallitto E, Gargiulo M, et al. Results of the endovascular abdominal aortic aneurysm repair using the Anaconda aortic endograft. J Vasc Surg 2014;60:1132–9.
[7] Rödel SGJJ, Zeebregts CJ, Meerwaldt R, et al. Incidence and treatment of limb occlusion of the anaconda endograft after endovascular aneurysm repair. J Vasc Endovasc Ther 2019;26:113–20.
[8] Hammond A, Hansrani V, Lowe C, et al. Meta-analysis and meta-regression analysis of iliac limb occlusion after endovascular aneurysm repair. J Vasc Surg 2018;68:1916–1924.e7.
[9] Faure EM, Becquemin JP, Cochennec F. Predictive factors for limb occlusions after endovascular aneurysm repair. J Vasc Surg 2015;61:1138–45.
[10] Mantas GK, Antonopoulos CN, Sfyroeras GS, et al. Factors predisposing to endograft limb occlusion after endovascular aortic repair. Eur J Vasc Endovasc Surg 2015;49:39–44.
[11] Georgakarakos E, Argyriou C, Schoretsanitis N, et al. Geometrical factors influencing the hemodynamic behavior of the AAA stent grafts: essentials for the clinician. Cardiovasc Intervent Radiol 2014;37:1420–9.
[12] Carroccio A, Faries PL, Morrissey NJ, et al. Predicting iliac limb occlusions after bifurcated aortic stent grafting: anatomic and device-related causes. J Vasc Surg 2002;36:679–84.
[13] Maleux G, Koolen M, Heye S, et al. Limb occlusion after endovascular repair of abdominal aortic aneurysms with supported endografts. J Vasc Interv Radiol 2008;19:1409–12.
[14] Guan X, Guan X, Martonen TB, et al. Simulations of flow in curved tubes. Aerosol Sci Technol 1997;26:485–504.
[15] Koenrades MA, Klein A, Leferink AM, et al. Evolution of the proximal sealing rings of the anaconda stent-graft after endovascular aneurysm repair. J Endovasc Ther 2018;25:480–91.
[16] Freyrie A, Gargiulo M, Rossi C, et al. Preliminary results of Anaconda™ aortic endografts: a single center study. Eur J Vasc Endovasc Surg 2007;34:693–8.
[17] Rödel SGJ, Geelkerken RH, Prescott RJ, et al. The Anaconda™ AAA stent graft system: 2-year clinical and technical results of a multicentre clinical evaluation. Eur J Vasc Endovasc Surg 2009;38:732–40.
[18] Klein A, Jan Renema WK, van der Vliet JA, et al. Motion calculations on stent grafts in AAA. In: Grundmann RT, ed., The Diagnosis, Screening and Treatment of Abdominal, Thoracoabdominal and Thoracic Aortic Aneurysms. Rijeka, Croatia: InTechOpen 2011:125–44.
[19] Klein A, van der Vliet JA, Oostveen LJ, et al. Automatic segmentation of the wire frame of stent grafts from CT data. Med Image Anal 2012;16:127–39.
[20] Koenrades MA, Struijs EM, Klein A, et al. Quantitative stent-graft motion in ECG-gated CT by image registration and segmentation: in vitro validation and preliminary clinical results. Eur J Vasc Endovasc Surg 2019;58:746–55.
[21] Schuurmann RCL, Kuster L, Slump CH, et al. Aortic curvature instead of angulation allows improved estimation of the true aorto-iliac trajectory. Eur J Vasc Endovasc Surg 2016;51:216–24.
[22] Harris P, Brennan J, Martin J, et al. Longitudinal aneurysm shrinkage following endovascular aortic aneurysm repair: a source of intermediate and late complications. J Endovasc Surg 1999;6:11–6.
[23] Di Achille P, Tellides G, Figueroa CA, et al. A haemodynamic predictor of intraluminal thrombus formation in abdominal aortic aneurysms. Proc R Soc A Math Phys Eng Sci 2014;470:20140163.
[24] Chuter TAM. Durability of endovascular infrarenal aneurysm repair: when does late failure occur and why? Semin Vasc Surg 2009;22:102–10.
[25] Lindblad B, Dias N, Malina M, et al. Pulsatile wall motion (PWM) measurements after endovascular abdominal aortic aneurysm exclusion are not useful in the classification of endoleak. Eur J Vasc Endovasc Surg 2004;28:623–8.
[26] Vos AWF, Wisselink W, Marcus JT, et al. Cine MRI assessment of aortic aneurysm dynamics before and

after endovascular repair. J Endovasc Ther 2003;10:433–9.
[27] Demanget N, Duprey A, Badel P, et al. Finite Element Analysis of the mechanical performances of 8 marketed aortic stent-grafts. J Endovasc Ther 2013;20:523–35.
[28] Itoga NK, Suh G-Y, Cheng CP. Stabilization of the abdominal aorta during the cardiac cycle with the sac-anchoring Nellix device. Ann Vasc Surg 2018;52. 312.e7–12.
[29] Lee K, Hossain S, Sabalbal M, et al. Explaining endograft shortening during endovascular repair of abdominal aortic aneurysms in severe aortoiliac tortuosity. J Vasc Surg 2017;65:1297–304.
[30] Harris PL, Buth J, Mialhe C, et al. The need for clinical trials of endovascular abdominal aortic aneurysm stent-graft repair: the EUROSTAR Project. J Endovasc Ther 1997;4:72–7.